Electronic Supplementary Material (ESI) for Journal of Materials Chemistry A.
This journal is © The Royal Society of Chemistry 2024

Supporting Information

Rapid Self-Healing and Superior Toughness in Ionically Crosslinked Polymer Ionogel and Strain Sensing Applications

Anil Kumar Padhan[a], Diksha Sharma[a], Tino S. Thomas[a], Aayushi Prakash Sinha[a], Adarsha Narayan Mallick[b], and Debaprasad Mandal*[a]

[a]Department of Chemistry, Indian Institute of Technology Ropar, Punjab 140001, India

[b]Department of Biomedical Engineering, Indian Institute of Technology Ropar, Punjab 140001, India

Experimental Section

Materials

Hexane, chloroform, and ethyl acetate are purified by simple distillation. Tetrahydrofuran, and diethyl ether were passed through neutral alumina followed by distillation over Na/benzophenone. Acetone was freshly dried over KOH and CaH_2 respectively followed by distillation. Acetonitrile and dichloromethane distilled over P_2O_5; and methanol over magnesium cake. Vinylimidazole (Alfa Aesar, 99.5%); 2,2'-azobis(2-methylpropionitrile) (AIBN) (Sigma Aldrich, 98%); polyphosphoric acid, (83% P_2O_5 basis), $Ca(NO_3)_2.4H_2O$ (99%), Urea (99.5%) from Spectrochem, India and NaCl (MERCK, 99%) were used as received. All polymers were vacuum dried at 60 °C and 2 × 10^{-3} mbar for 4 h before performing each test. The microwave-assisted reactions were carried out in Anton Paar Multiwave Pro and Monowave 200 instruments. Aqueous solutions were prepared with deionized water (Millipore).

Characterizations

NMR spectra were recorded using a JEOL JNM-ECS400 spectrometer at ambient probe temperatures and referenced as follows: ^{1}H: residual H from internal $CDCl_3$ (δ = 7.26 ppm); DMSO-d_6 (δ = 2.50 ppm); ^{13}C: internal $CDCl_3$ (δ = 77.1 ppm); DMSO-d_6 (δ = 40.4 ppm); FT-IR spectra were recorded as neat with ATR on Bruker Tensor-27, with Zinc Selenide window spectrometer in the range of 600-4000 cm^{-1}.

Size exclusion chromatography (SEC) measurements. Molar masses (M_n) and dispersity of the polymers **1** were measured from size exclusion chromatography (SEC) with triple-detection GPC from Agilent 1260 GPC/SEC MDS and PolarGel L (PL1117-6830) 300 × 7.5 mm columns. Water/methanol (50 vol%) containing LiBr (1%) was used as an eluent with a flow rate of 1.0 mL/min. The entire SEC system was thermostated at 40 °C. The system was calibrated using linear poly(ethylene glycol) (PEG) of narrow polydispersity index as an internal standard. The typical sample concentration and injection volume were 10 mg/mL and 100 µL respectively. The results were processed using the corresponding Agilent software referring to RI signal.

Thermal Analysis. The thermal decomposition temperature was recorded in N_2 atmosphere using an alumina pan by thermogravimetric analysis (TGA) technique on a "TGA/DSC1" instrument from Mettler Toledo with SDTA sensor and data were analyzed in STAR^e software (version 12.1). Thermal stability was investigated by heating from 25 °C to 800 °C at a heating rate of 10 °C/min at 40 mL/min N_2 (99.999%) flow. Each sample was tested at least three times and the error limit is <2%. The phase-transition temperatures were recorded by differential scanning calorimeter (DSC) using a DSC1/700W with HSS8 sensor instrument (Mettler Toledo) with Huber TC100MT Intercooler and Olympus microscope attachments using aluminum pan with pin as reference. The DSC measurements were performed through a 5 steps heat-cool-heat-cool-heat program to ensure the phase transitions and the details are as follows: step 1: heating from 20 °C to 200 °C at a rate of 40 °C/min and held for 2 min; step 2: cooling from 200 °C to 20 °C at a rate of 40 °C/min and held for 2 min; step 3: heating from 20 °C to 200 °C at a rate 40 °C/min and held for 2 min; step 4: cooling from 200 °C to 10 °C and held for 2 min; step 5: heating from 20 °C to 200 °C. These polymers were thermally annealed by repeatedly cycling and/or holding the samples at 20 °C temperatures for varying period of time to allow a complete crystallization.

Rheology

The rheological test and viscosity measurements were carried out under atmospheric conditions on Anton Paar Rheometer (MCR102) with SN81403820; FW3.80; Slot (3,-1); Adj (9,0)d, measuring system: PP25-SN34217; [d=0.3 mm], angular frequency ω=10 rad/s Peltier temperature control. The typical size of ionogel was 20.0 mm in diameter with 3.0 mm thickness approximately. Self-healing performances were measured by rheological failure-recovery tests by applying large amplitude strains to break the gel integrity followed by monitoring gel recovery. Initial viscoelastic properties were measured at 5% strain and 10 rad/s angular frequency. After 1 min, the strain was ramped until 200% in 1 min to ensure gel network disruption. After the loss of gel integrity, the initial test conditions were restored to follow the time-dependent recovery of gel integrity for 1 min. Six failure-recovery cycles were applied consecutively, and the recovery was quantified by comparing the storage modulus (G'), loss modulus (G''), and damping factor (Tanδ) before and after each rupture. All measurements were performed at least three times at constant temperature (25 °C) and under controlled atmospheric moisture.

Microwave Plasma Atomic Emission Spectroscopy (MPAES)

The Ca-ion was investigated by MPAES of model 4120MP-AES. All the polymers were digested in HNO_3 and diluted using Millipore water. The calibration curve was generated using Ca-ion standard from a calibration range of 1-5 ppm and a correlation coefficient limit=0.999. All measurements were repeated at least 5 times for each sample.

EDS Analysis

EDS analysis was conducted on the powder specimen using a JEOL JSM-6610 LA (JEOL, Japan) with Oxford Inca X-act as the detector. Integrated JEOL Analysis Station software was used to collect and analyze the X-ray data. The coated sample itself was fixed onto an aluminum stage, ensuring that the carbon-coated surface was in good contact with the holder. All analyses (spot and line) were performed under high vacuum conditions. The

Tensile Test

Tensile measurements were conducted on a Tinius Olsen H50KS with serrated calipers using a closing pressure of 10 psi and a strain speed of 1 mm/min. Sheets of the network thin film of a dog-bone-shaped polymer of PVIMH-PPA/ PVIM-PPA-Ca samples with gauge lengths 30.0 mm, 4.0 mm thickness. and 3.0 mm width were measured with a caliper and used for tensile testing before and after the healing experiments according to ASTM standard D638-14 Type V. All measurements were repeated at least 3 times for each sample. We have also studied the mechanical properties of the ionogel **3c** after keeping under 80% humidity, and at different temperatures of 120 °C, 80°C and -25 °C.

Self-healing properties of Ionogels

The ionogel was cut into two pieces, and then the fractured surfaces of the two pieces were simply brought into contact with each other without any further operation to observe the self-healing phenomenon immediately and all the images were recorded using digital camera.

Evaluation of self-healing efficiency

The original ionogels were cut into half using blades. The separated ionogel surfaces were re-contacted. The healing efficiency (HE) is defined by the following equation:

$$HE = \sigma_H/\sigma_O \times 100\ \%$$

in which σ_H and σ_O are the storage modulus (G'), tensile stress, elongation break (%), Young's Modulus of the self-healed ionogel and original Ionogel respectively. The average values and errors were calculated from at least three independent samples for each specimen.

Tearing test

The tearing test was performed to measure tearing energy (fracture of toughness) using EZ Test Universal Testing Instrument EZ-LX-HS MODEL, SHIMDZU. Samples of 3 mm (w) in thickness and 50 mm (L) × 7.5 mm (d) with the initial notch length of 20 mm were used. The two arms of the Ionogel were clamped tightly by metal plates to prevent the sample from slipping during the tearing test. To make sure the advanced crack along the central line through the entire sample, the two arms were set perpendicular to the object surface of the clamps. The upper clamp was stretched at a constant stretch speed of 1 mm/min until the crack advanced through the entire sample, and the corresponding tearing force F and stretched displacement or extension L were recorded during the test. The tearing energy T was calculated at a constant tearing force F using the relation $T = 2F/w$, where w is the thickness of the sample.

Ionic Conductivity and strain sensing

Impedance spectroscopy was conducted using a platinum four probe by Autolab frequency response analyzer connected to Autolab potentiostat/galvanostat. Samples were initially sandwiched in a Teflon spacer of 4 mm diameter and 2 mm thickness between two Pt-electrodes. The ionic conductivities were measured at room temperature before and after the self-healing experiment. Strain-sensing experiments for monitoring human motions were detected by connecting the electrodes of an electrochemical workstation to the ends of ionogel with copper tape and fixing the ionogel to the various parts of the body such as knees, arms, throat, and fingers. The ionogel was directly attached to the skin of the body parts

and multiple bending-stretching processes were undertaken to record the rate of change of resistance-time curve. The resistance changes of the ionogel were obtained by using an electrochemical workstation (Metrohm M204). The gauge factor (GF) is defined as GF = $[(R - R_0)/R_0]/\varepsilon = (\Delta R/R_0)/\varepsilon$, where R_0 and R are the resistances of the original and stretched ionogel, respectively, and ε is the strain of the ionogel ($\Delta L/L$). Thickness of the ionogel **3c** was 1.0 mm during the measurement. All the experiments were performed at ambient conditions. The human motion studies were conducted following the informed consent of the participants. Ethical approval was not required in this case.

Table S1: Self-healing mechanisms and conditions, healing efficiency, toughness, fracture energy, and ionic conductivity of various ionogels.

	Materials used	Self-healing condition	Healing efficiency (%)	Gauge Factor (g)	Toughness (MJ/m^3)	Fracture energy (kJ/m^2)	Conductivity (mS/cm)	References
1	**PVIM-PPA-Ca (3c)**	**Immediate**	**≥87**	**2.18, 5.54**	**>41.0**	**4.7**	**0.0593**	**This work**
2	**PVIM-PPA (2)**	**Immediate**	**~90**	**-**	**>43.0**	**4.1**	**0.0125**	**This work**
3	P[IL-EO/IL-OH] TFSI	Room temp. for 2 h	100	-	0.64 ± 0.02	-	0.131	1
4	P[VBIM]Zn_xBr_y	Water drops and at 40 °C for 12 h	-NA-	3.1, 4.4, 6.4	130.3	243.4	0.02	2
5	LA/TA/$AlCl_3$ polymer network-[EMIm]OAc	Room temp. for 15 h	90.1	0.42, 0.64, 0.81	1.3	-	0.037	3
6	PACMO-$[N_{4111}]NTf_2$	60 ºC oven for 30 min	67	1.1, 2.3	4.9	-	1.5	4
7	P(AAm-co-AA)-[EMIM]ES	60 °C for 60s	60 (@24 h)	-	-	~24	-	5
8	PVA-[BMIm]Zn_xBr_y	-NA-	-NA-	-	1947±52	505	0.8	6
9	P(MEA-co-IBA)-LiTFSI	Room temp. for 24 h	30-40	2.02, 4.0, 6.0	-	21.7	0.0528	7
10	PDMAA-PAMPS-[EMIm]TFSI	100 ºC for 20 min	100	3.5, 9.8	19	87	0.011	8
11	P(ATFE-co-NIPAm)-[EMIm]TFSI	Underwater for 2 h	96	0.81, 1.67	3.9	8.4	~2	9
12	PUA-P(ACMO)-[EMIM]TFSI	80 °C for 6 h	95.5	0.98, 1.56	-	-	0.75	10
13	P(TFEA-co-Aam)-[EMIM]TFSI	30 °C for 12 h	99	0.83, 1.38, 1.85	3.6	-	2.27	11
14	P[VBIM]BF_4-$BMIMBF_4$	80 °C for 5 min	100	0.99, 1.85	39.2	-	1.5	12

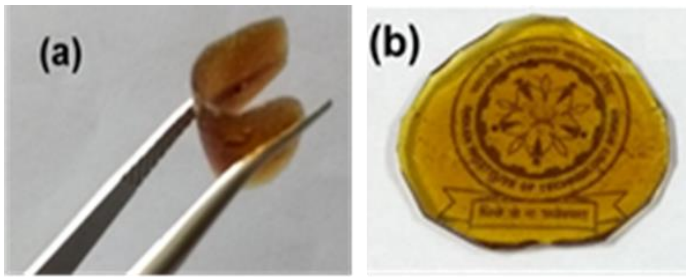

Figure S1. Image of model ionic polymers PVIM-PPA **(2);** (a) Flexible, (b) Transparent thin film with a thickness of 1.0 mm.

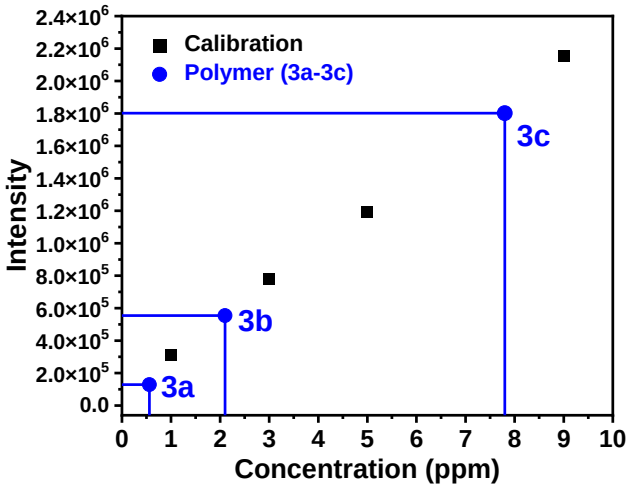

Figure S2. MP-AES analysis for polymer **3a-c** Calibration curve

Table. S2 MPAES results of polymer of polymer **3a-3c of Ca (393 nm)**

Polymer	**3a**	**3b**	**3c**
Ca-ion (ppm)	0.56+0.15	2.1±0.05	7.8±0.05

From MPAES, 7.8 ppm Ca-ion in 100 mL solution of 5 mg polymer; equivalent to 1.56 wt%. (2.21 wt% as Ca-ion taken for **3c** preparation and from MPAES Ca-ion found is 1.56 wt%)

Ca^{2+} = [(40/236.1)*0.472 g]/3.62 g(total mass taken)x100 % =0.08 /3.62 x100 %= 2.2 wt.%

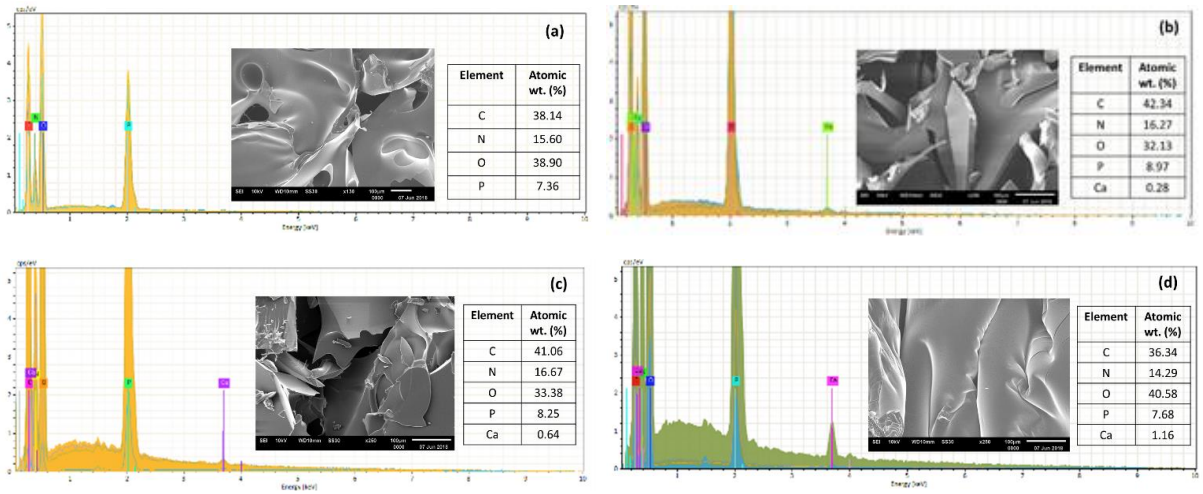

Figure S3. SEM-EDS analyses of (a) poly**mers 2**, (b) **3a,** (c) **3b,** and (d) **3c** with Ca-ion atomic wt% from SEM-EDS analysis along with illustrating their typical compositions corresponding ratios calculated from the atomic % of P relative to C and/or N.

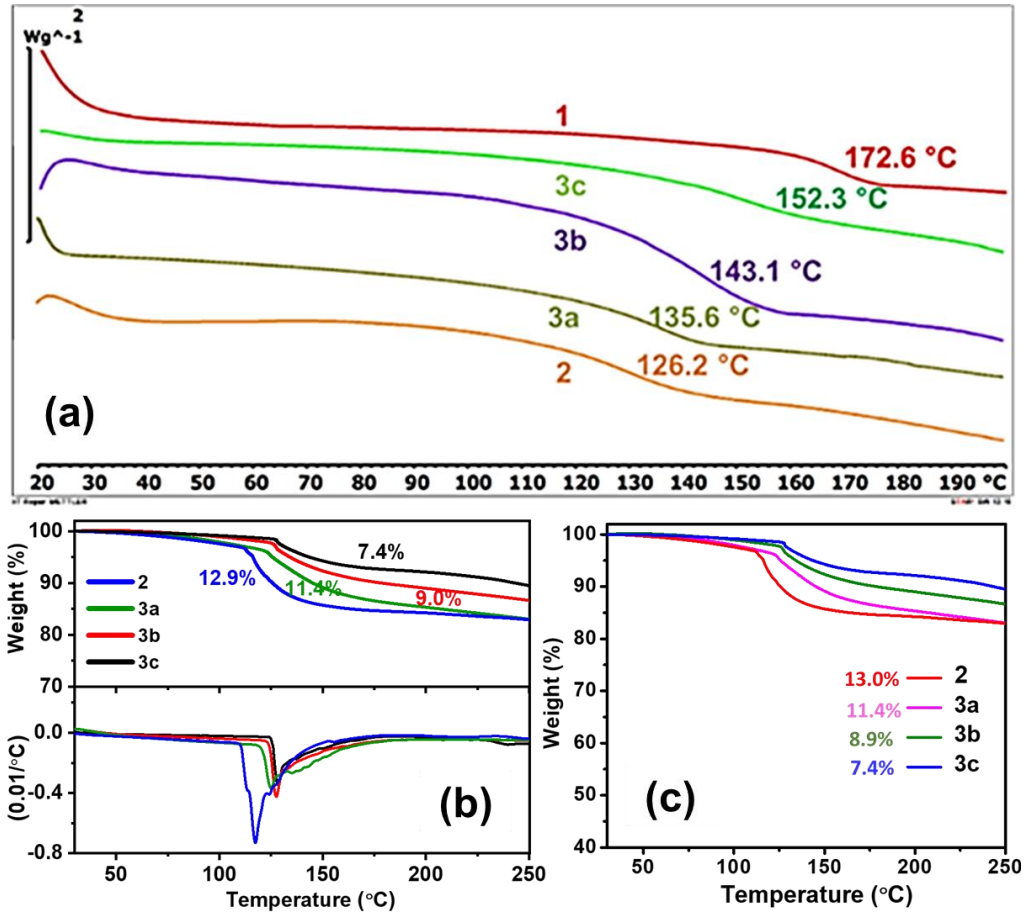

Figure S4. (a) DSC curve of freeze-dried polymers (b) TGA and DTG curves of ionogel used for evaluation of water content. (c) The water content of the ionogels after kept at ambient conditions for one week.

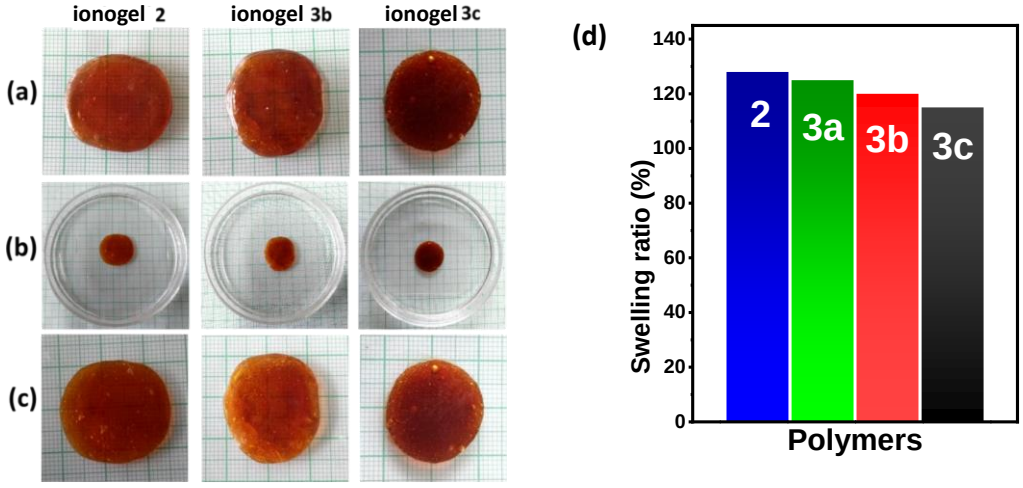

Figure S5. Saline stability test photographs of **2, 3b** and **3c,** (a) Virgin ionogels, (b) dipped in 3 M NaCl (c) after 48 h in 3 M NaCl, (d) the corresponding swelling ratio (118-128%).

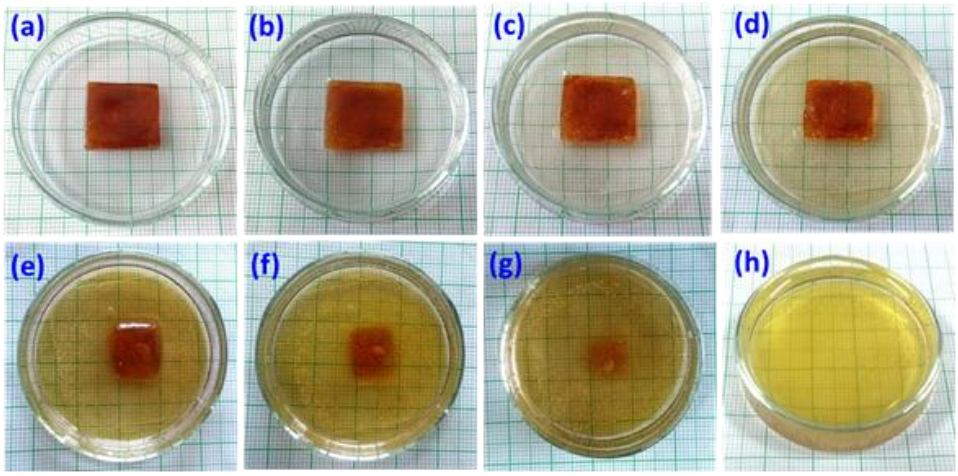

Figure S6. (a-g) Photographs of the ionogel **2** in 3 M NaCl at 60 °C every 1 h interval, and (h) complete dissolution of 2 after 10 h.

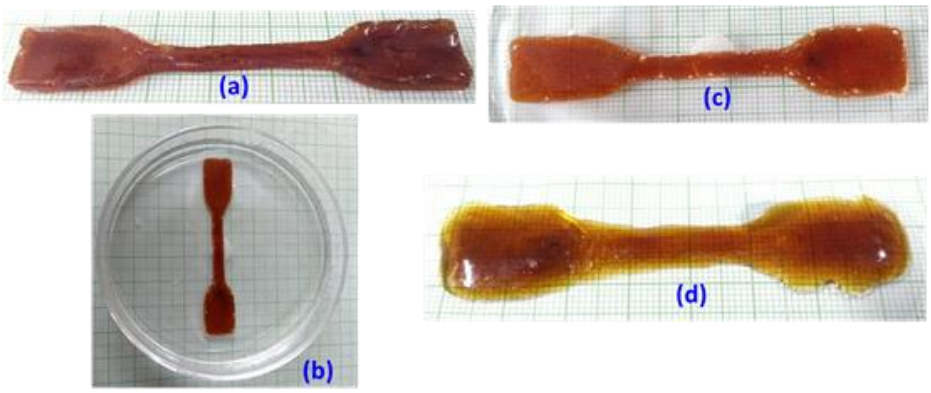

Figur S7. Photographs during the urea solution stability tests of **2**; (a) virgin ionogel, (b) dipped in 3 M urea solutions, (c) after 12 h in urea solutions, and (d) after 48 h in urea solutions.

Good stability of these ionogels in saline environments and urea solutions highlights the roles of interpenetrating network of polymer entanglement with ionic and hydrogen bonds interactions within the ionogel network. The polymer network of PVIM and self-association of $[PVIMH]_n^+$ and $[PPA]^-$ by the ionic and H-bonding networks (established due to the protonation of PVIM with PPA), is crosslinked and formed an interpenetrating network. Simple electrostatic interactions and H-boding networks are typically susceptible to the saline water and Urea solution. However, the tolerance of these ionogels in saline water and urea solution proves the efficacy of the highly crosslinked, strong interpenetrating chain entanglement network, which effectively inhibits the swelling of the ionogel and protects the locking effect of the chain entanglement, preventing immediate destruction. However, the network undergoes degradation over the long term in urea solution and under heating in saline water.

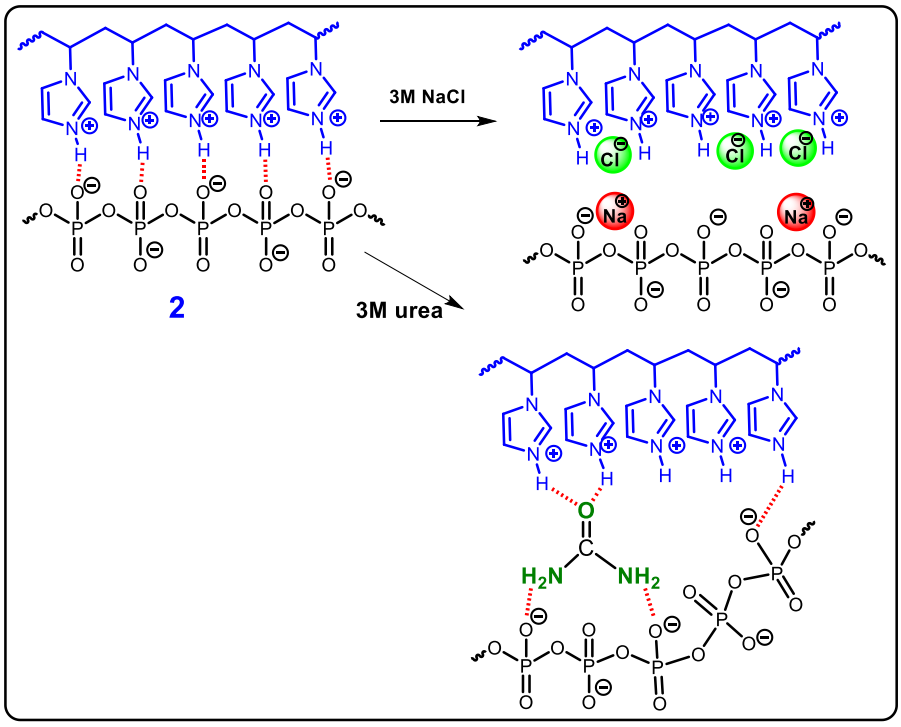

Scheme S1. Competitive electrostatic and H-bonding interactions between $PVIMH^+/PPA^-$ vs NaCl and Urea solution

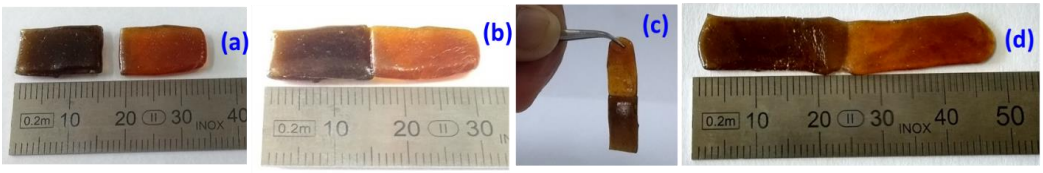

Figure S8. (a) Pieces of fresh ionogel **2** and methylene blue dye-doped **2** (dark brown); and, (b) self-healing after joining for few seconds, (c) self-hanging after healing and (d) stretched after healing of **2** dye-doped.

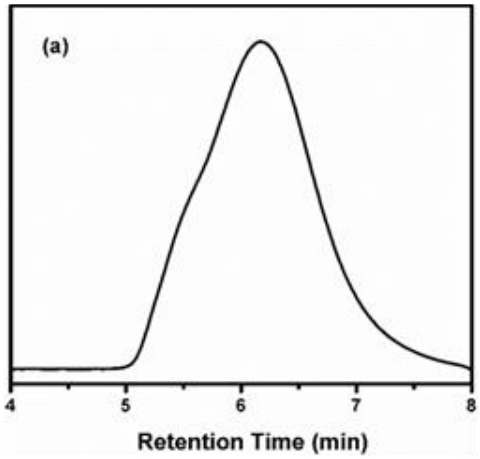

Figure S9. GPC traces of polymer PVIM **(1)**

Table. S3 GPC results of polymer **PVIM (1)**

Polymer	M_n	M_w	PDI
1	11,100	18,900	1.70

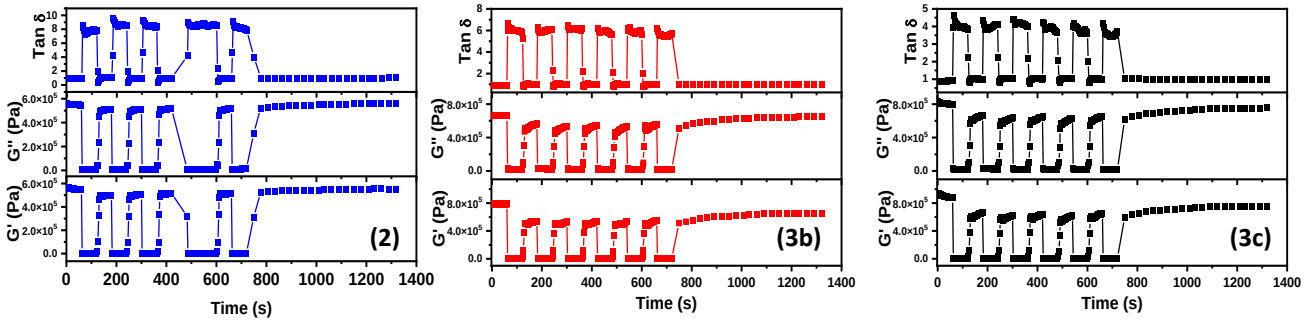

Figure S10: (a) Self-healing efficiency from rheology failure-recovery tests where gel failure was induced by a sudden increase in 200% strain at 25 °C and a constant angular frequency of 10 rad/s. The recovery of the storage modulus (G'), loss modulus (G''), and tan δ for each cycle of (a) **2**, (b) **3b**, (c) **3c**.

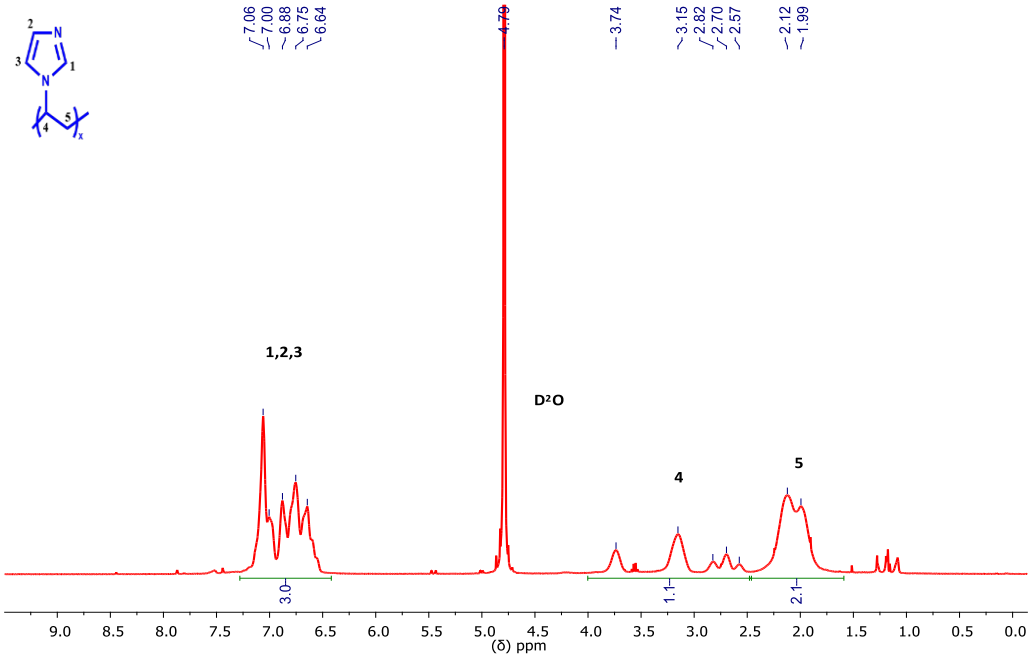

Figure S11. ^{1}H NMR of **1** in D_2O.

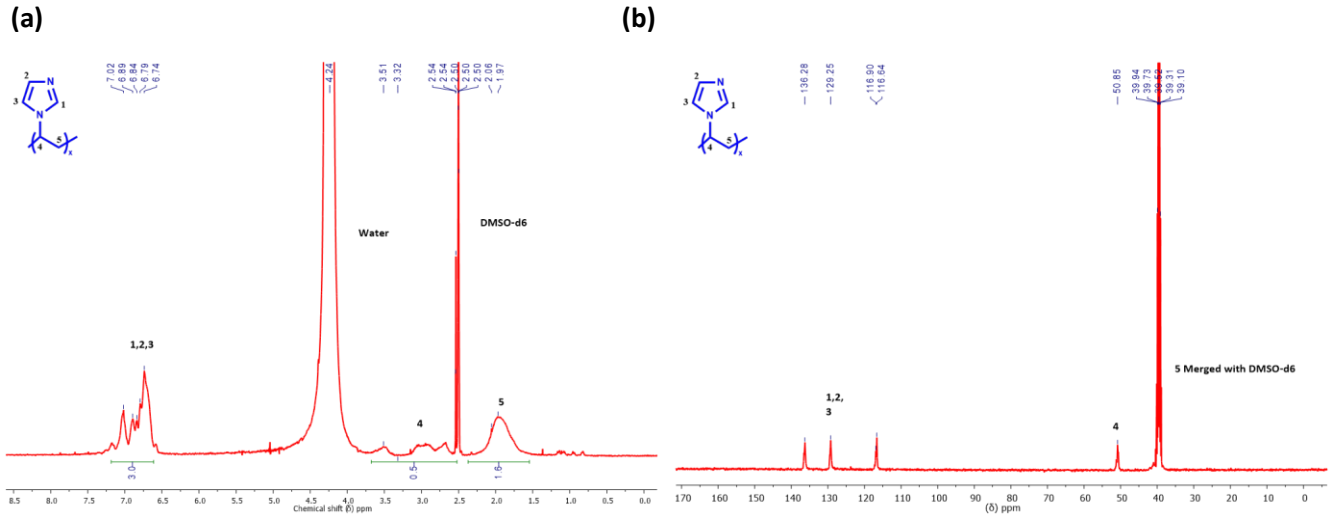

Figure S12. (a) ^{1}H NMR (b) ^{13}C of **1** in DMSO-d_6.

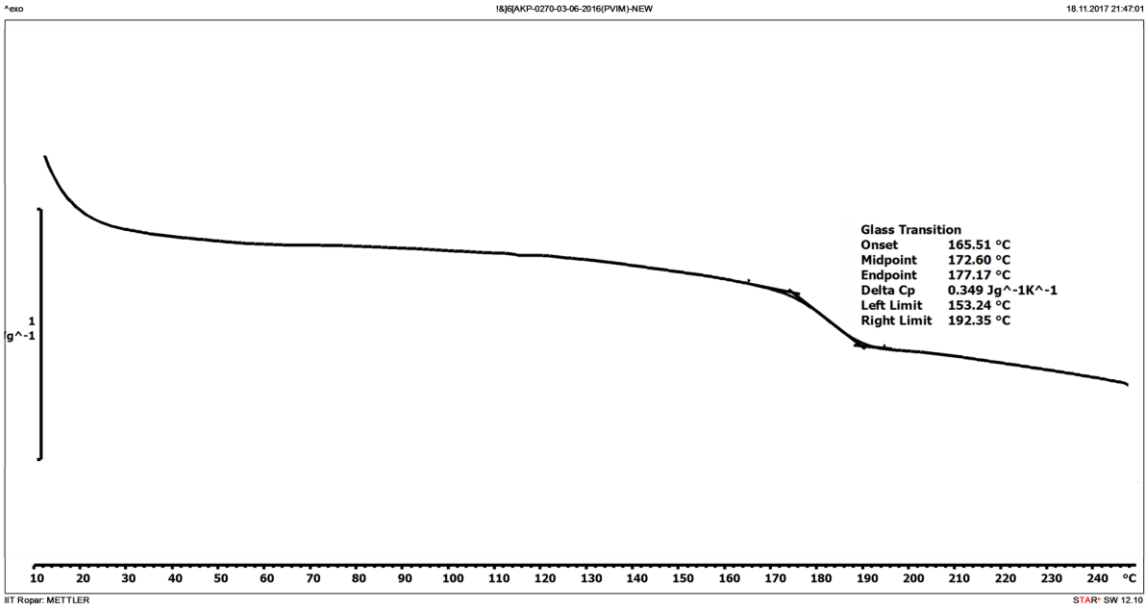

Figure S13: DSC curve of PVIM (**1**)

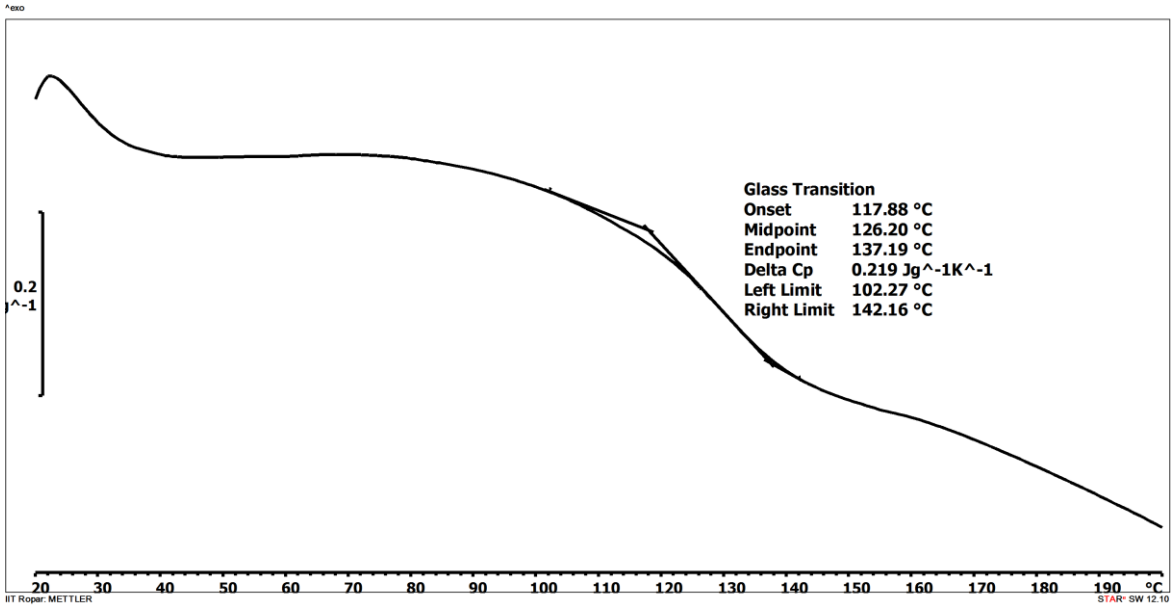

Figure S14: DSC curve of PVIM-PPA **(2)**

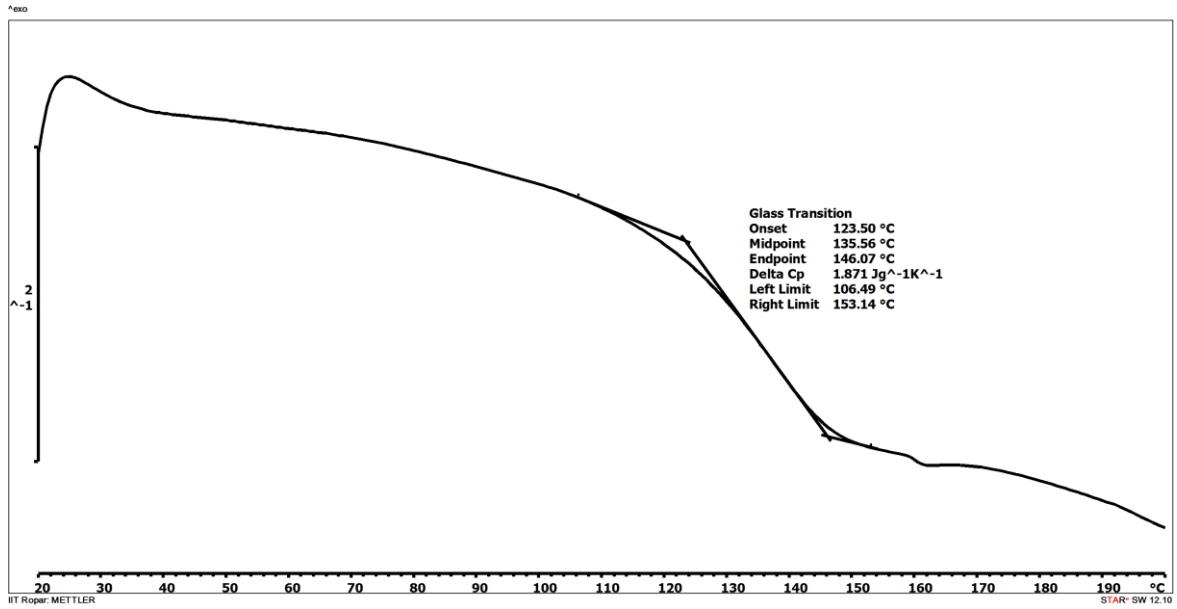

Figure S15: DSC curve of PVIM-PPA-Ca **(3a)**

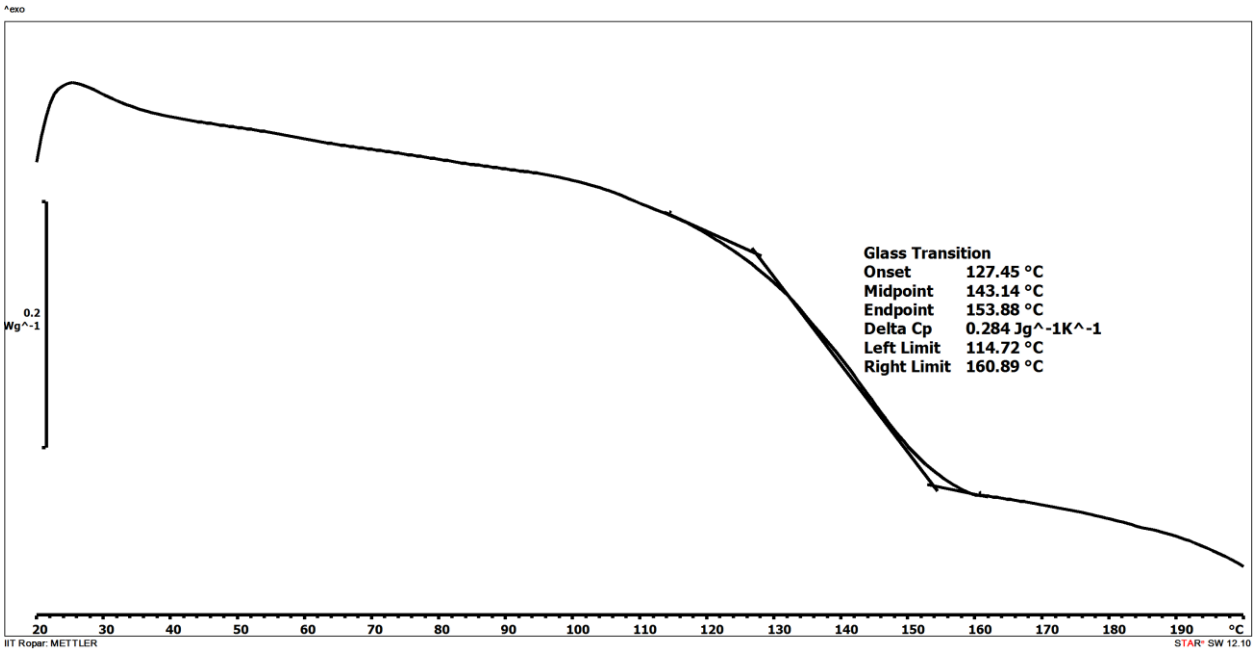

Figure S16: DSC curve of PVIM-PPA-Ca **(3b)**

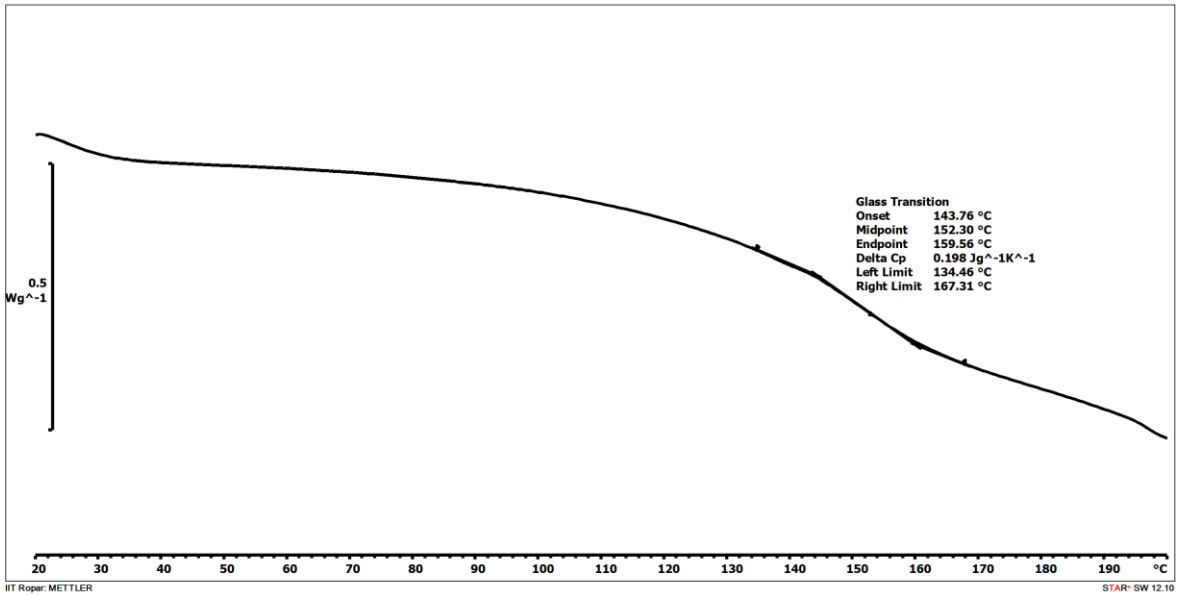

Figure S17: DSC curve of PVIM-PPA-Ca **3b.**

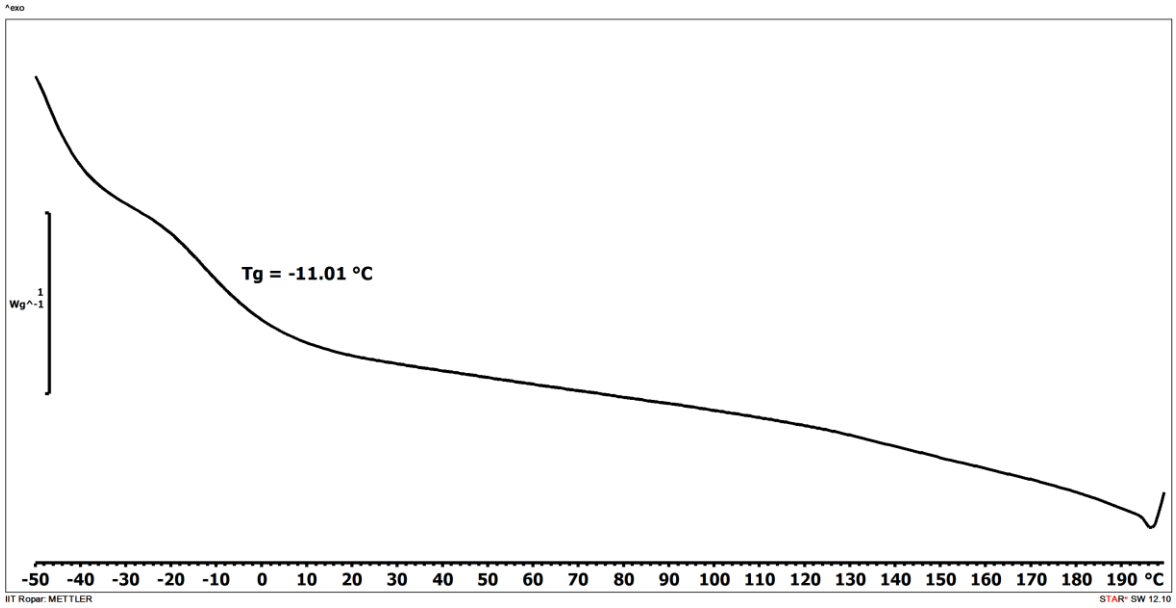

Figure S18: DSC curve of **PPA**

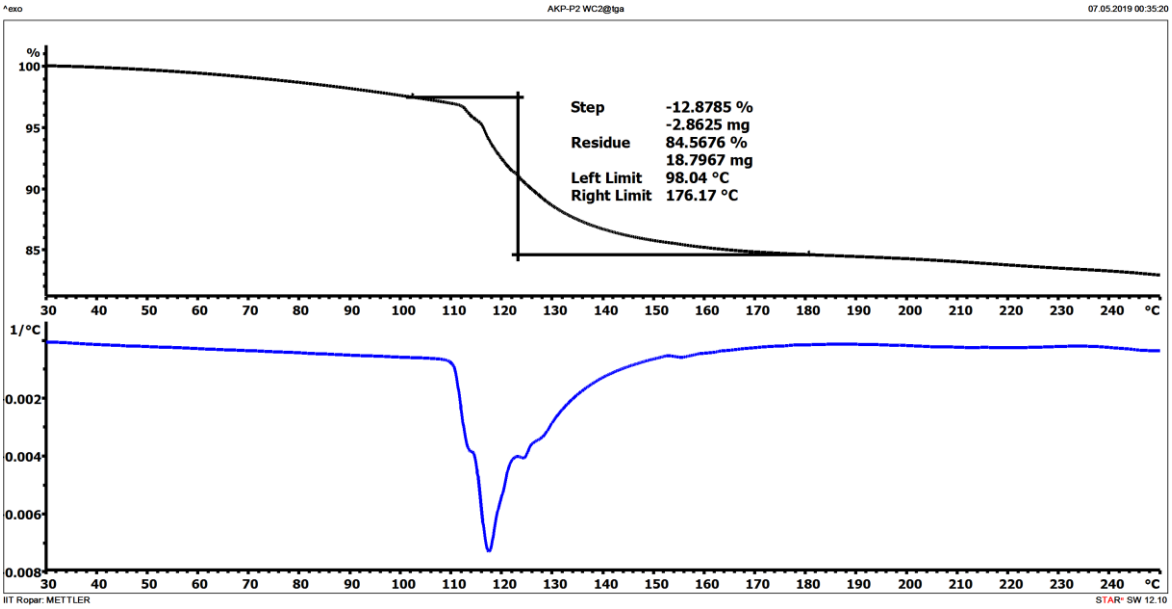

Figure S19: TGA curve of **2** used for evaluation of water content.

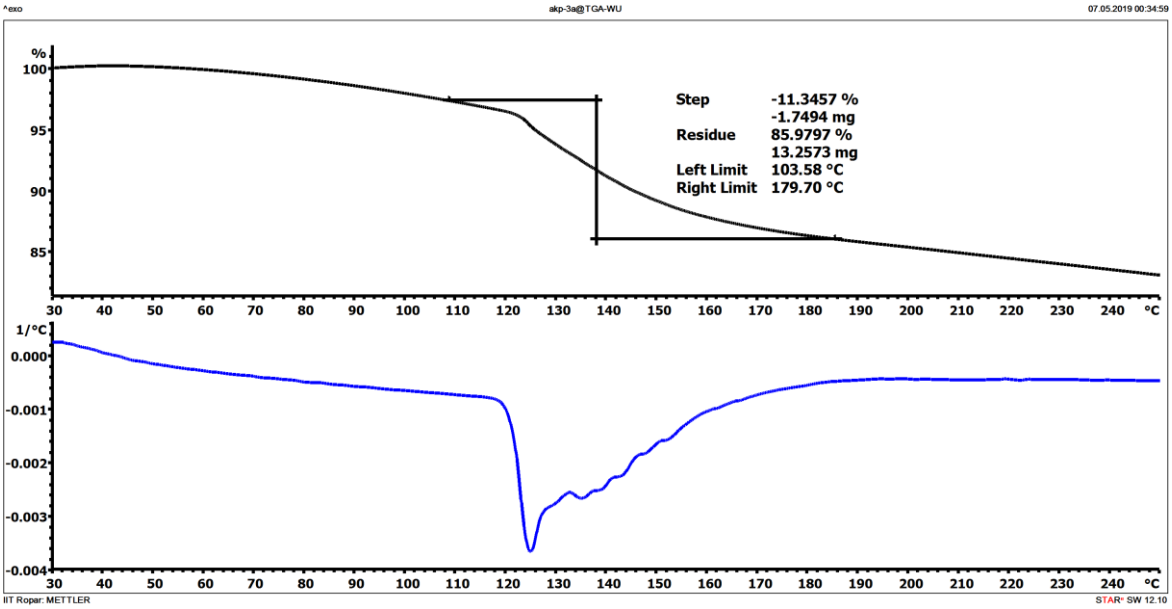

Figure S20: TGA curve of **3a** used for evaluation of water content.

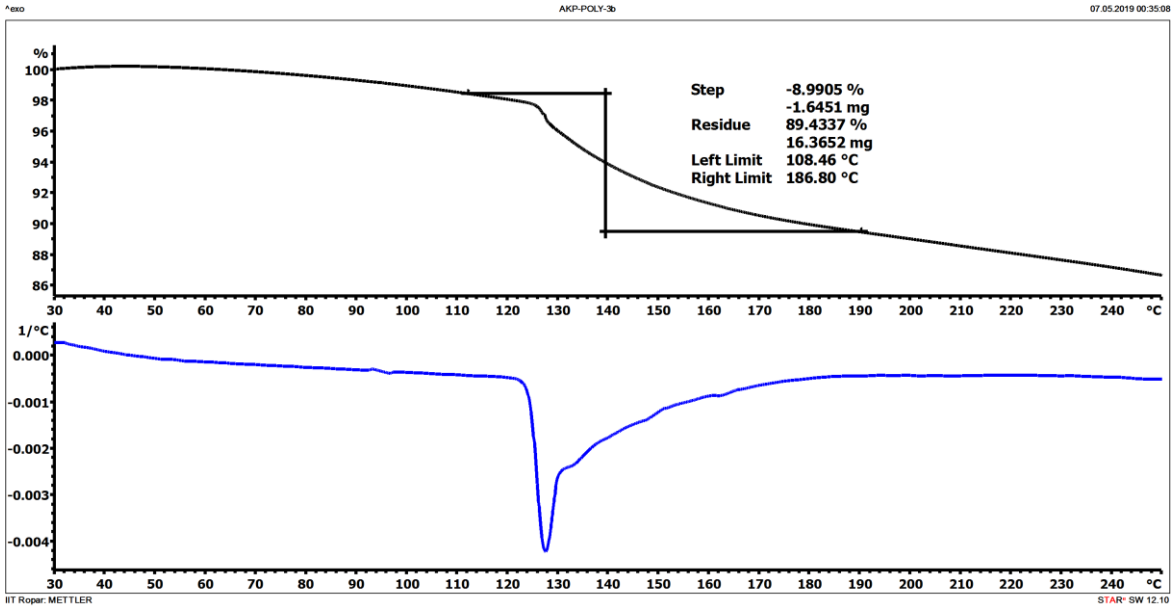

Figure S21. TGA curve of **3b** used for evaluation of water content.

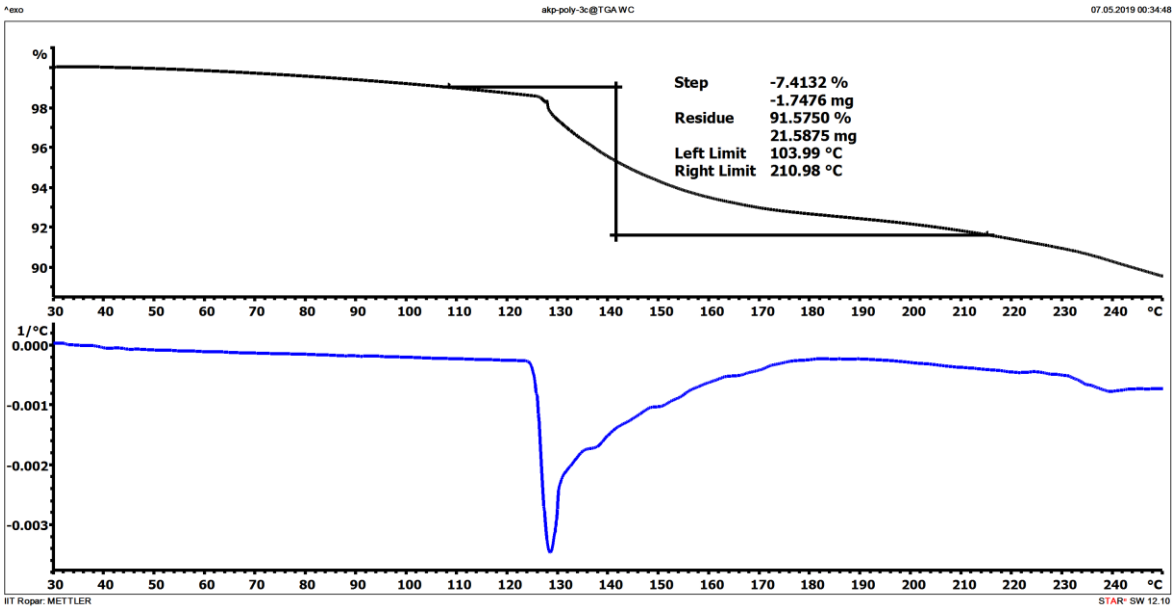

Figure S22: TGA curve of **3c** used for evaluation of water content.

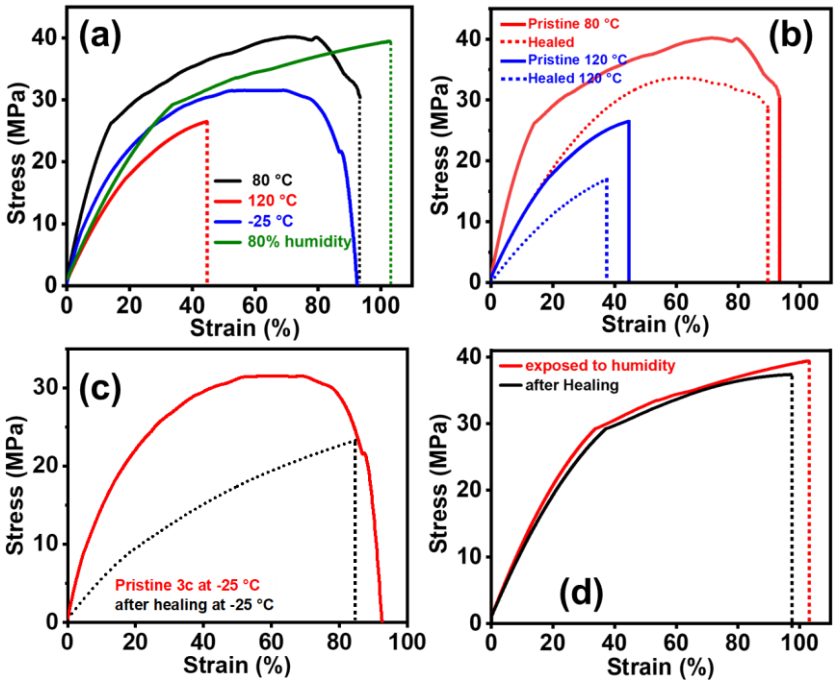

Figure S23: Stress-strain curves of 3c (a) kept at -25 °C, 80 °C and 120 °C for 24 h and under 80% humidity for three days; after self-healing of fractured material during tensile test (b) samples from 80 and 120 °C of ionogel 3c (c) self-healing at -25 °C (d) healing under 80% humidity condition.

Table S4. Tensile properties of **3c** kept at different temperatures, humid condition, and after self-healing of fractured materials during tensile test.

Ionogel (3c)	Young's modulus (MPa)	Ultimate stress (MPa)	Elongation at break (%)	Toughness (MJ/m3)	Healing efficiency
Pristine 3c (at ambient atm.)	4.1±0.1	39±1	110±2	41.4±2	
Pristine **3C** (kept at 80 °C)	3.3±0.8	40.0±2	105±2	30.5±2	
Healed after fracture	2.4±0.8	29.0±2	93±2	23.1±2	96%
Pristine **3C** (kept at 120 °C)	1.9 ±1	26.0±3	44±5	7.53±4	
Healed after fracture	1.3±1	16.1±3	37±4	3.4±4	83%
Pristine **3C** (Kept at -25 °C)	2.9±0.8	33.1±2	103±2	23.0±3	
Healed (at –25 °C)	1.5±0.8	23.3±2	84±2	12.3±3	91%
Pristine (80% humidity)	2.0±0.8	39±1	103±2	30.8±2	
Healed (80% humidity)	1.8±0.8	37±1	97±2	26.5±2	96%

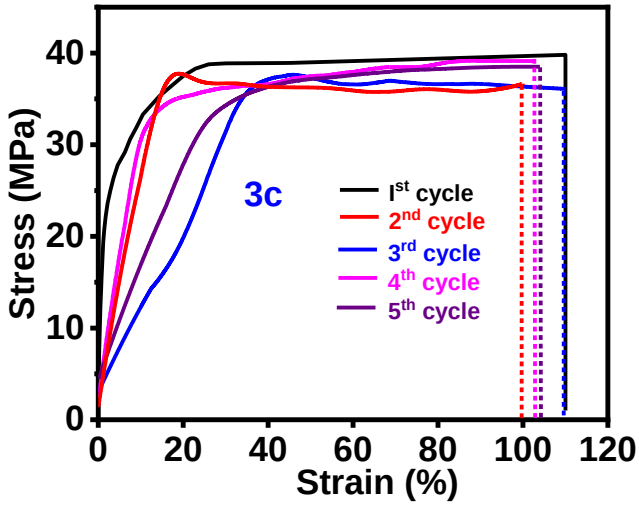

Figure S24: Repeatable self-healing stress-strain curves of the polymeric material 3c with healing time of 1 min.

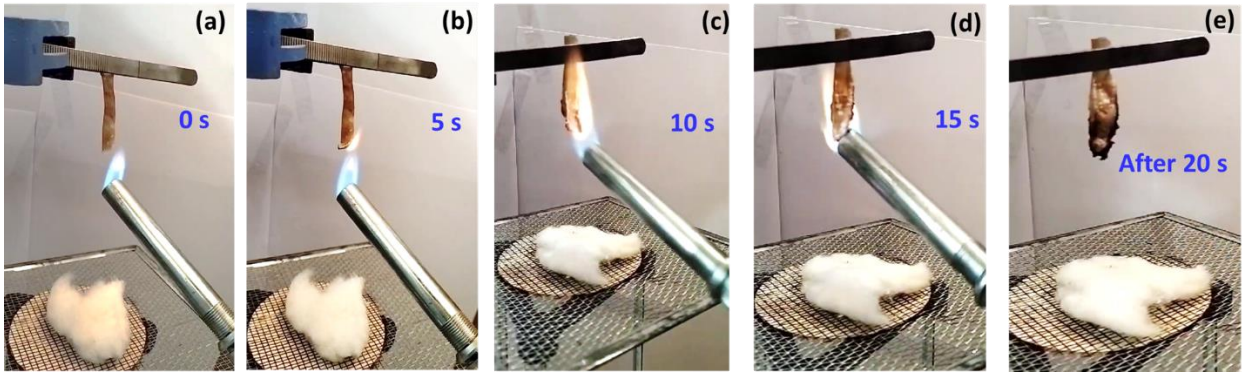

Figure S25. Flame resistant UL-94 test of **3c**

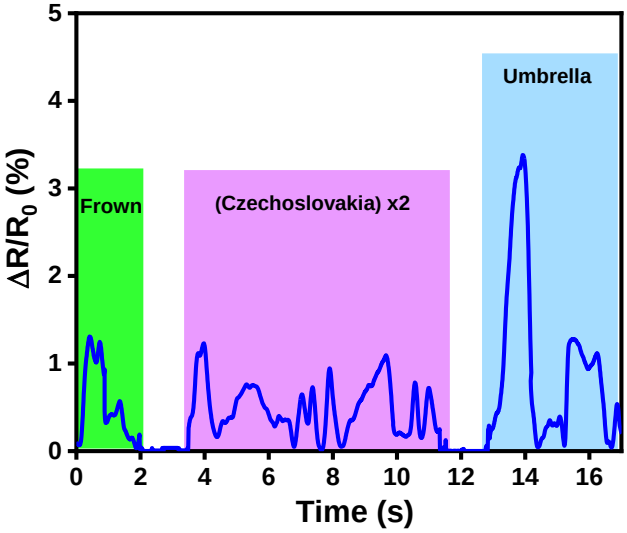

Figure S26: Real-time monitoring of the PVIM-PPA-Ca **(3c)** ionogel-based wearable strain sensor when speaking different words.

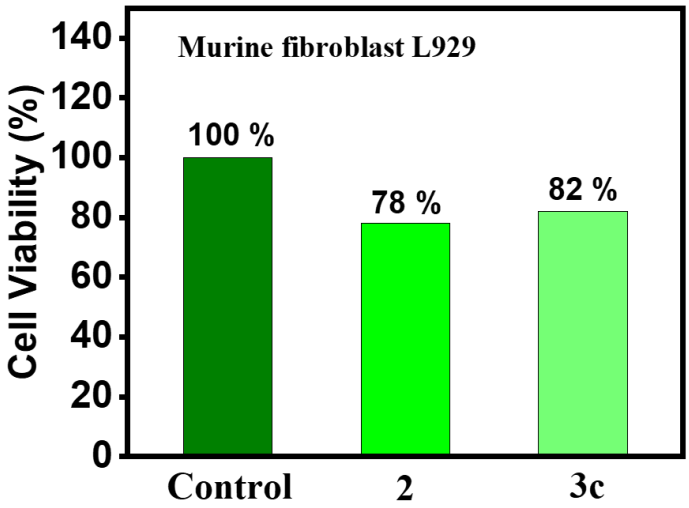

Figure S27. Cell viability studies of murine fibroblast (L929) cells as control and incubated with material **2** and **3c**.

References:

1. X. Qu, W. Niu, R. Wang, Z. Li, Y. Guo, X. Liu and J. Sun, *Mater. Horiz.*, 2020, **7**, 2994-3004.
2. L. Li, X. Wang, S. Gao, S. Zheng, X. Zou, J. Xiong, W. Li and F. Yan, *Adv. Mater.*, 2023, 2308547.
3. C. Dang, F. Peng, H. Liu, X. Feng, Y. Liu, S. Hu and H. Qi, *J. Mater. Chem. A*, 2021, **9**, 13115-13124.
4. J. Tie, Z. Mao, L. Zhang, Y. Zhong and H. Xu, *Adv. Funct. Mater.*, 2023, DOI:, 2307367.
5. M. Wang, P. Zhang, M. Shamsi, J. L. Thelen, W. Qian, V. K. Truong, J. Ma, J. Hu and M. D. Dickey, *Nat. Mater.*, 2022, **21**, 359-365.
6. W. Li, L. Li, Z. Liu, S. Zheng, Q. Li and F. Yan, *Adv. Mater.*, 2023, **35**, 2301383.
7. B. Yiming, Y. Han, Z. Han, X. Zhang, Y. Li, W. Lian, M. Zhang, J. Yin, T. Sun, Z. Wu, T. Li, J. Fu, Z. Jia and S. Qu, *Adv. Mater.*, 2021, **33**, 2006111.
8. W. Li, L. Li, S. Zheng, Z. Liu, X. Zou, Z. Sun, J. Guo and F. Yan, *Adv. Mater.*, 2022, **34**, 2203049.
9. Y. Zhao, F. Wang, J. Liu, D. Gan, B. Lei, J. Shao, W. Wang, Q. Wang and X. Dong, *ACS Appl. Mater. Interfaces*, 2023, **15**, 28664-28674.
10. M. Zhang, X. Tao, R. Yu, Y. He, X. Li, X. Chen and W. Huang, *J. Mater. Chem. A*, 2022, **10**, 12005-12015.
11. L. Xu, Z. Huang, Z. Deng, Z. Du, T. L. Sun, Z.-H. Guo and K. Yue, *Adv. Mater.*, 2021, **33**, 2105306.
12. T. Li, F. Liu, X. Yang, S. Hao, Y. Cheng, S. Li, H. Zhu and H. Song, *ACS Appl. Mater. Interfaces*, 2022, **14**, 29261-29272.